

# Electron conduction along quantizing magnetic fields in neutron star crusts

## II. Practical formulae

A.Y. Potekhin<sup>1,2\*</sup> and D.G. Yakovlev<sup>1</sup>

<sup>1</sup>A.F. Ioffe Physical-Technical Institute, 194021, St-Petersburg, Russia

<sup>2</sup>Nordita, Blegdamsvej 17, DK-2100 Copenhagen Ø, Denmark

Received 26 October 1995 / Accepted 17 February 1996

**Abstract.** We derive practical expressions for a rapid and accurate evaluation of electric and thermal conductivities and thermopower of degenerate relativistic electrons along quantizing magnetic fields in outer neutron star crusts. We consider the electron Coulomb scattering on ions in liquid matter, as well as on high-temperature phonons or charged impurities in solid matter. We propose also a reasonable semi-quantitative treatment of low-temperature phonons. The transport properties are expressed through the energy dependent effective electron relaxation time averaged over electron energies. We calculate this relaxation time, using the theoretical formalism of the previous work, obtain accurate fitting expressions, and propose an efficient energy averaging procedure. We create a computer code which calculates the longitudinal transport properties of degenerate electrons in strong magnetic fields for any parameters of dense stellar matter of practical interest. We analyse quantum oscillations of the transport coefficients versus density at various temperatures and magnetic fields.

**Key words:** stars: neutron – dense matter – magnetic fields

### 1. Introduction

Transport properties of neutron star crusts are important for studies of thermal evolution (cooling) of neutron stars, evolution of their magnetic fields, etc. For instance, the heat in the outer crusts of magnetized neutron stars is mainly transported by electrons along the magnetic fields. As a rule, the electrons in the crust are strongly degenerate, and they may be relativistic. The main electron scattering mechanisms are the Coulomb scattering on ions in the liquid phase, and the scattering on phonons or charged impurities in the solid phase; the magnetic field can quantize electron motion.

Send offprint requests to: A.Y. Potekhin (Ioffe Institute)

\* e-mail: palex@astro.ioffe.rssi.ru

In the present work we study the electron transport properties in the outer crusts of neutron stars along quantizing magnetic fields. The problem has been considered earlier by several authors. The first were Canuto and his colleagues in 1970s; the results were summarized by Canuto & Ventura (1977). An adequate kinetic equation for the electron distribution function was proposed by Yakovlev (1980), and used for calculating the transport coefficients by Yakovlev (1980, 1984), Hernquist (1984), Van Riper (1988) and Schaaf (1988). Although much work has been done, these studies are not fully complete. First, the approach based on the distribution function formalism is not invariant: the results depend slightly on the choice of the electron wave functions (due to the spin degeneracy) in the magnetic field. Second, the results are not easy for practical use. Third, the previous studies neglected the Debye–Waller reduction of electron-phonon scattering rate in solid magnetized matter, although the importance of the Debye–Waller factor was demonstrated by Itoh et al. (1984, 1993) for the non-magnetic case.

Recently Potekhin (1996, hereafter Paper I) has developed an invariant formalism of the longitudinal electron conduction problem based on the spin polarization density matrix of the electrons. The results of Paper I have been compared with those obtained using the traditional methods with various electron basis functions. The latter methods are simpler for calculations, while the density matrix formalism enables one to choose which basis is more adequate at given parameters of stellar matter. Paper I has presented also efficient numerical techniques for calculating the electron transport coefficients including the Debye–Waller factor and demonstrated that this factor is much more significant when the field is strongly quantizing.

In this paper we obtain practical formulae for a simple and rapid evaluation of the longitudinal transport coefficients using the theory developed in Paper I.

### 2. Physical conditions

We consider degenerate layers of an outer neutron star crust (at densities  $\rho \lesssim 4 \times 10^{11} \text{ g cm}^{-3}$ , below the neutron drip). Matter

of these layers consists of electrons and ions. We study not too low densities (see below), at which the electrons are nearly free, and the ionization is complete due to the high electron pressure. The ions give the major contribution into the density while the electrons – into the pressure. For simplicity, we mainly consider one component plasma of ions (=nuclei ( $A, Z$ )); the electron and ion number densities are related as  $n_e = Zn_i$ . A comprehensive study of thermodynamic properties of magnetized neutron star crusts has been performed recently by Rönigvaldsson et al. (1993) using the Thomas–Fermi approximation. Since we avoid low densities, we base our consideration on the approximation of free electrons. This will enable us to evaluate the transport properties of matter. We will include the effects of non-ideality of electrons in a phenomenological manner in Sects. 5 and 6.

Let  $\mu$  be the electron chemical potential (including the electron rest-mass energy,  $mc^2$ ). The domain of strongly degenerate electrons we are interested in corresponds to  $T \ll T_F$ , where  $T_F = (\mu - mc^2)/k_B$  is the degeneracy temperature and  $k_B$  is the Boltzmann constant. If  $(\mu - mc^2) \ll mc^2$ , then the electron gas is non-relativistic, while for  $\mu \gg mc^2$  it becomes ultra-relativistic.

In the absence of the magnetic field, one has the familiar result

$$n_e = \frac{1}{\pi^2 \hbar^3} \int_0^\infty f(\varepsilon) p^2 dp, \quad (1)$$

where

$$f(\varepsilon) = \left[ \exp\left(\frac{\varepsilon - \mu}{k_B T}\right) + 1 \right]^{-1} \quad (2)$$

is the Fermi–Dirac distribution function, and  $\varepsilon = c\sqrt{(mc)^2 + p^2}$  is the electron energy. In the case of strong degeneracy, one has  $\mu \approx \mu_0$ , where

$$\mu_0 = \sqrt{m^2 c^4 + c^2 p_{F0}^2}, \quad p_{F0} = \hbar(3\pi^2 n_e)^{1/3}, \quad (3)$$

and  $p_{F0}$  is the field-free electron Fermi momentum ( $p_{F0}/(mc) \approx 1.009(\rho_6 Z/A)^{1/3}$ ,  $\rho_6$  being density in units of  $10^6 \text{ g cm}^{-3}$ ). The appropriate degeneracy temperature is plotted in Fig. 1 by short-dashed line. For small  $\rho$  and  $T$ , the effects of incomplete ionization and electron gas non-ideality become important. This domain is shown schematically by the short-dashed line  $N$ . The line corresponds to  $\bar{\varepsilon} = |\varepsilon_a|$ , where  $\bar{\varepsilon}$  is the mean energy per electron in the free electron gas, and  $\varepsilon_a$  is the mean energy per electron for isolated atoms in the Thomas–Fermi approximation (e.g., Landau & Lifshitz 1976).

Let the magnetic field  $B$  be directed along the  $z$ -axis. We shall use the Landau gauge of the vector potential:  $\mathbf{A} = (-By, 0, 0)$ . Quantum states of a free electron can be labelled by four quantum numbers  $(p_x, p_z, n, s)$ , where  $p_x$  determines the  $y$ -coordinate of the electron guiding center,  $y_B = p_x/(m\omega_B)$ ,  $p_z$  is the longitudinal electron momentum,  $n=0, 1, 2, \dots$  enumerates the Landau levels, and  $s$  is a spin variable. Here  $\omega_B = eB/(mc)$  is the electron cyclotron frequency, and  $(-e)$  is the electron charge. The ground Landau level  $n = 0$  is non-degenerate with

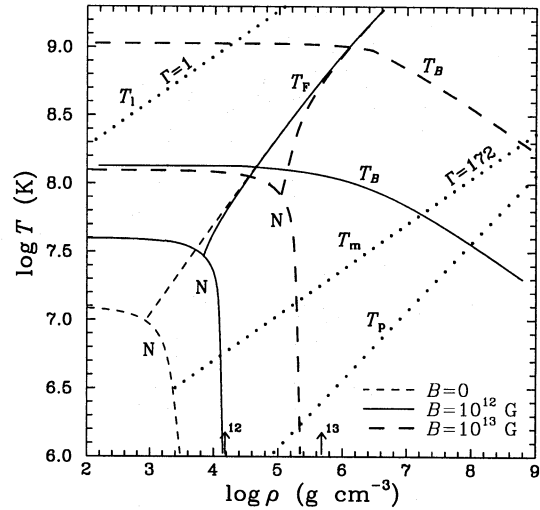


**Fig. 1.**  $\rho - T$  diagram of  $^{56}\text{Fe}$  matter for several magnetic field strengths.  $T_F$  – electron degeneracy temperature,  $T_1$  – ion coupling temperature ( $\Gamma = 1$ ),  $T_m$  – melting temperature,  $T_p$  – ion plasma temperature,  $T_B$  – electron quantization temperature; arrows indicate strongly quantizing densities  $\rho_B$ . Lines  $N$  restrict the low- $T$  low- $\rho$  domain of incomplete ionization and electron gas non-ideality.  $T_F$ ,  $T_B$ , and  $N$  curves depend on the magnetic field. Dashes show the curves for  $B = 0$ , solid lines for  $B = 10^{12}$  G, and thick long-dash lines for  $B = 10^{13}$  G.

respect to spin while the excited levels  $n > 0$  are doubly degenerate. Various sets of electron basic wave functions are analysed, e.g., in Paper I. An energy  $\varepsilon$  of a relativistic electron in the magnetic field is

$$\begin{aligned} \varepsilon &= \varepsilon_n \equiv E mc^2 \\ &= \sqrt{m^2 c^4 + c^2 p_z^2 + 2mc^2 \hbar \omega_B n}, \end{aligned} \quad (4)$$

where  $E$  is the natural dimensionless energy.

The number density of free electrons in a magnetic field is

$$\begin{aligned} n_e &= \frac{m\omega_B}{(2\pi\hbar)^2} \int_{-\infty}^{+\infty} dp_z \sum_{n,s} f(\varepsilon_n) \\ &= \int_{mc^2}^{\infty} \mathcal{N}_e(\varepsilon) \left( -\frac{\partial f}{\partial \varepsilon} \right) d\varepsilon, \end{aligned} \quad (5)$$

$$\mathcal{N}_e(\varepsilon) = \frac{2m\omega_B}{(2\pi\hbar)^2} \sum_s \sum_{n=0}^{n(E)} p_n(\varepsilon). \quad (6)$$

Here  $p_n(\varepsilon) \equiv mcP_n(E)$  is the largest  $z$ -momentum of an electron with energy  $\varepsilon$  at a given Landau level,  $n(E) = \text{Int}(\nu)$  is the highest Landau level occupied by an electron with energy  $\varepsilon$ ,

$$P_n(E) = \sqrt{E^2 - 1 - 2bn}, \quad \nu = (E^2 - 1)/(2b), \quad (7)$$

$\text{Int}(\nu)$  is integer part of  $\nu$ , and  $b$  is the dimensionless magnetic field expressed in units of the ‘critical field’  $B_c$  ( $\hbar\omega_{Bc} = mc^2$ ),

$$b = \frac{B}{B_c}, \quad B_c = \frac{m^2 c^3}{e\hbar} = 4.414 \times 10^{13} \text{ G}. \quad (8)$$

Mass density  $\rho$  equals  $\rho \approx m_i n_i \approx (A/Z)m_u n_e$ , where  $m_i$  is the ion mass,  $m_u = 1.660 \times 10^{-24}$  g is the atomic mass unit, and  $A/Z$  is the number of baryons per electron. Equation (5) determines  $n_e$  as a function of  $T$ ,  $\mu$  and  $B$ .

Simple analysis of Eq. (5) yields the following. Strongly degenerate electrons populate the only ground Landau level when density is not too high,  $\rho < \rho_B$ , where  $\rho_B = 2.07 \times 10^6 b^{3/2}(A/Z)$  g cm $^{-3}$ . In this case the Fermi momentum is

$$p_F = \frac{2\pi^2 \hbar^2 n_e}{m\omega_B} = \frac{2}{3b} p_{F0} \left( \frac{p_{F0}}{mc} \right)^2. \quad (9)$$

In the domain of  $\rho \ll \rho_B$  the magnetic field strongly reduces the electron Fermi energy and widens the region of incomplete ionization and electron gas non-ideality (Yakovlev 1984, Hernquist 1984, Van Riper 1988), as shown in Fig. 1 by solid and long-dashed lines. In this case, lines  $N$  correspond to  $\bar{\varepsilon} = |\varepsilon_a|$ , where  $\varepsilon_a$  depends on  $B$  (Rögvaldsson et al. 1993).

If  $B$  is fixed, then  $\mu$  increases with  $\rho$ , and degenerate electrons populate higher Landau levels  $n$ . If  $\rho \gg \rho_B$ , many Landau levels are populated, and the Fermi energy is almost independent of  $B$  ( $p_F \approx p_{F0}$ ).

It is convenient to introduce the temperature

$$T_B = \frac{\hbar\omega_B^*}{k_B} \approx 1.34 \times 10^8 B_{12} \frac{mc^2}{\varepsilon^*} \text{ K}, \quad (10)$$

where  $\omega_B^* = eBc/\varepsilon^*$  is the gyrofrequency of an electron with the typical energy  $\varepsilon^* = \max(\bar{\varepsilon}, \mu)$ , and  $B_{12} = B/(10^{12} \text{ G})$ . When  $T \gg T_B$  the electrons occupy many Landau levels for any  $\rho$  due to high thermal energy. In this case the thermal widths of the Landau energy levels ( $\sim k_B T$ ) are higher than the inter-level spacing, and the magnetic field acts as *non-quantizing*, regardless of the electron degeneracy.

In the domain of  $T \lesssim T_B$  and  $\rho < \rho_B$  (separated into the subdomains of degenerate and non-degenerate electron gas) the electrons populate mostly the ground Landau level. In this domain, the magnetic field is *strongly quantizing*, and it affects significantly all properties of matter (e.g., Van Riper 1988, Yakovlev & Kaminker 1994).

Finally, in the domain of  $T \lesssim T_B$  and  $\rho \gg \rho_B$  the electrons are degenerate and populate many Landau levels but the inter-level spacing exceeds  $k_B T$ . Then the magnetic field is *weakly quantizing*. It does not affect noticeably the bulk properties (pressure, electron chemical potential) determined by all the electron Fermi sea but it affects the transport properties determined by thermal electrons near the Fermi level.

The state of ions can be characterized by the ion coupling parameter

$$\Gamma = \frac{Z^2 e^2}{ak_B T} = 2.275 \frac{Z^2}{T_7} \left( \frac{\rho_6}{A} \right)^{1/3}, \quad (11)$$

where  $a = [3/(4\pi n_i)]^{1/3}$  is the ion sphere radius, and  $T_7$  is temperature in units of  $10^7$  K.

At high  $T$ , when  $\Gamma \ll 1$ , the ions form a classical Boltzmann gas. With decreasing  $T$ , the gas gradually (without any phase

transition) becomes a Coulomb liquid. The liquid is formed (Hansen 1973) at  $\Gamma \approx 1$ , i.e., at  $T \approx T_1$  (Fig. 1). The liquid solidifies into the Coulomb crystal (Nagara et al. 1987) at  $\Gamma = 172$  ( $T = T_m$ ). According to Fig. 1, we always have strongly coupled Fe ions, if electrons are degenerate ( $T_1 > T_F$ ). However, for light ions,  $T_1$  can be lower than  $T_F$ .

At low  $T$ , zero-point ion vibrations become important in ion motion. These effects are especially pronounced if  $T \ll T_p$ , where

$$T_p = \hbar\omega_p/k_B \approx 7.832 \times 10^6 (Z/A)\rho_6^{1/2} \text{ K}, \quad (12)$$

and  $\omega_p = \sqrt{4\pi Z^2 e^2 n_i/m_i}$  is the ion plasma frequency. The amplitude of zero-point vibrations is commonly much smaller than the typical inter-ion distance,  $a$ . With increasing  $\rho$ , the amplitude-to- $a$  ratio becomes larger, so that the vibrations can prevent crystallization at high  $\rho$  (Mochkovitch & Hansen 1979, Ceperley & Alder 1980). This effect is especially pronounced for H and He. Note that the Debye temperature of the Coulomb bcc crystal is  $T_D = 0.45T_p$  (Carr 1961).

We assume that the magnetic fields do not affect the properties of the ion plasma component, for instance, the phonon spectrum of the crystal. This is so (e.g., Usov et al. 1980) if  $\omega_B = ZeB/(m_i c) \ll \omega_p$ , i.e., if  $B \ll 10^{14} \sqrt{\rho_6}$  G.

### 3. Transport properties

#### 3.1. Electron scattering mechanisms

The electron transport properties are determined by the electron scattering mechanisms. Consider three important cases when the electron scattering is almost elastic (an energy transfer in a collision event is  $\ll k_B T$ ): (i) the Coulomb scattering on ions in the liquid or gaseous phase ( $T > T_m$ , Fig. 1), (ii) the scattering on high-temperature phonons ( $T_D \lesssim T < T_m$ ); (iii) the Coulomb scattering on charged impurities in the lattice (important for  $T \ll T_D$ ). The impurities represent ions of charge  $Z_{\text{imp}} \neq Z$  immersed accidentally in lattice sites. Accordingly, our results cover a wide range of temperatures.

The electron-ion scattering can approximately be described (e.g., Yakovlev 1984) by the Debye-screened Coulomb potential. Its Fourier image  $U(\mathbf{q})$  is given by

$$|U_{\text{ion}}(\mathbf{q})|^2 = \left( \frac{4\pi Z e^2}{q^2 + q_s^2} \right)^2, \quad (q_s^{\text{ion}})^2 = q_i^2 + q_e^2, \quad (13)$$

where  $q_s$  is an effective screening wavenumber (inverse screening length),  $q_i$  and  $q_e$  are, respectively, the ion and electron screening wavenumbers. According to Yakovlev & Urpin (1980) and Yakovlev (1984),

$$q_i^{-2} = (2a/3)^2 + r_D^2, \quad q_e^2 = 4\pi e^2 (\partial n_e / \partial \mu), \quad (14)$$

where  $r_D$  is the Debye ion radius,  $r_D = v_i/\omega_p$ ,  $v_i = \sqrt{k_B T/m_i}$  is the thermal ion velocity. The Debye radius dominates ( $q_i \approx 1/r_D$ ) in the gaseous regime  $T \gg T_1$ , while  $q_i \approx 1.5/a$  in the most important case of strongly coupled ion liquid ( $T_m < T \lesssim$

$T_1$ ). Equation (14) allows us to reproduce the  $B = 0$  transport properties using the model potential (13) instead of the exact plasma-screened Coulomb potential.

For the scattering on high-temperature phonons, one has (e.g., Paper I)

$$|U_{\text{ph}}(\mathbf{q})|^2 = \left( \frac{4\pi Z e^2}{q} \right)^2 \frac{r_T^2}{3} \exp[-2W(\mathbf{q})], \quad (15)$$

where  $r_T^2 = u_{-2} a^2 / \Gamma$  is the mean squared thermal displacement of ions from their lattice sites,  $u_{-2}$  is a numerical factor determined by the phonon spectrum ( $u_{-2} = 13.0$  for the body-centered cubic (bcc) lattice, see, e.g., Mochkovitch & Hansen 1979),  $e^{-2W}$  is the Debye–Waller factor,  $2W(\mathbf{q}) \approx (r_T q)^2 / 3$ . Theoretical formalism for incorporating this factor into the transport properties of magnetized matter was developed in Paper I. Note that Eq. (15) is valid for  $T_D \lesssim T < T_m$ .

The scattering on phonons remains to be the dominant electron scattering mechanism at lower temperatures,  $T \ll T_D$ . The low- $T$  phonon scattering is inelastic (electron energy transfer in a collision is  $\sim k_B T$ ), and, strictly speaking, it cannot be described using the formalism of Paper I. However this scattering can approximately (semi-quantitatively) be treated as elastic (Yakovlev & Urpin 1980, Raikh & Yakovlev 1982) as long as the Umklapp processes dominate over the normal processes of electron-phonon interaction. The Umklapp processes are known to be most important at high temperatures, under typical conditions in neutron star crusts. However they are “frozen out”, and the electron scattering becomes essentially inelastic. For instance, for nonquantizing fields, this happens at  $T \ll T_U \sim T_p Z^{1/3} e^2 / (\hbar v_F) \approx [Z^{2/3} + 0.98(A/\rho_6)^{2/3}]^{1/2} (T_p/137)$ , where  $v_F$  is the electron Fermi velocity. We propose to extend the formalism of high-temperature phonons to  $T \ll T_D$  and obtain, thus, the reliable estimates of low-temperature transport properties at  $T_U \lesssim T \ll T_D$ . For this purpose, as can be shown, for instance, from the results of Raikh & Yakovlev (1982) and Baiko & Yakovlev (1995), the scattering potential (15) should be modified in two ways. First, the pre-exponent factor  $r_T^2$  should be replaced by  $r_{T1}^2 = r_T^2 G(t)$ , where  $G(t) = t / \sqrt{t^2 + t_0^2}$  describes the reduction of thermal ion displacements at low  $T$ ,  $t \equiv T/T_p$ , and  $t_0 \sim 0.1$  is a numerical parameter ( $t_0 = 0.132$  for the bcc lattice). Second, one should remind that the Debye–Waller factor is determined by the total (thermal + zero point) mean squared ion displacement  $r_{T2}^2$  which reduces to the thermal squared displacement  $r_T^2$  at high  $T$ . Thus we should replace  $r_T^2$  by  $r_{T2}^2 = r_T^2 \{1 + \exp(-9.1t)[u_{-1}/(2u_2 t)]\}$  in the Debye–Waller exponent (Baiko & Yakovlev 1995) for it to be accurate at low  $T$ . In this case,  $u_{-1}$  is another parameter of the phonon spectrum ( $u_{-1} = 2.800$ , for the bcc lattice). The above modifications do not violate the formalism of Paper I.

Finally, the scattering on impurities corresponds to (e.g., Yakovlev & Urpin 1980)

$$|U_{\text{imp}}(\mathbf{q})|^2 = \left[ \frac{4\pi(Z_{\text{imp}} - Z)e^2}{q^2 + q_s^2} \right]^2. \quad (16)$$

In this case the screening wavenumber is  $(q_s^{\text{imp}})^2 = q_e^2 + q_{\text{imp}}^2$ , where  $q_e$  is given by Eq. (14), and  $q_{\text{imp}}$  is an inverse impurity correlation length. The scattering on impurities is similar to that on ions. This scattering acts at  $T < T_m$ , just as the scattering on phonons, but actually it dominates at very low  $T$  (see Yakovlev & Urpin 1980).

### 3.2. Transport coefficients

Let  $\mathcal{E}$ ,  $\partial\mu/\partial z$  and  $\partial T/\partial z$  be, respectively, weak and locally constant electric field, electron chemical potential gradient, and temperature gradient along  $\mathbf{B}$ . They induce the electron electric and thermal currents with the current densities  $\mathcal{J}$  and  $\mathcal{Q}$ :

$$\begin{aligned} \mathcal{J} &= \sigma \left( \mathcal{E} + \frac{1}{e} \frac{\partial\mu}{\partial z} \right) + \beta \frac{\partial T}{\partial z}, \\ \mathcal{Q} &= -\beta T \left( \mathcal{E} + \frac{1}{e} \frac{\partial\mu}{\partial z} \right) - \lambda \frac{\partial T}{\partial z}. \end{aligned} \quad (17)$$

Here  $\sigma$  is the longitudinal electric conductivity, while  $\beta$  and  $\lambda$  are two other auxiliary transport coefficients. The appearance of  $\beta$  in the expressions for  $\mathcal{J}$  and  $\mathcal{Q}$  reflects the Onsager symmetry principle. For practical use, the expressions (17) can be rewritten as

$$\mathcal{E} + \frac{1}{e} \frac{\partial\mu}{\partial z} = \frac{\mathcal{J}}{\sigma} - \alpha \frac{\partial T}{\partial z}, \quad \mathcal{Q} = -\alpha T \mathcal{J} - \kappa \frac{\partial T}{\partial z}, \quad (18)$$

where

$$\alpha = \beta/\sigma, \quad \kappa = \lambda - T(\beta^2/\sigma) \quad (19)$$

are, respectively, the longitudinal thermopower, and thermal conductivity. The transport coefficients  $\sigma$ ,  $\beta$ , and  $\lambda$  are convenient for calculation (see Eq. (22) below) while  $\sigma$ ,  $\alpha$  and  $\kappa$  directly enter the equations which govern the distributions of temperature and magnetic field in neutron stars (e.g., Urpin & Yakovlev 1980). The coefficients  $\sigma$ ,  $\kappa$ , and  $\alpha$  determine fully the electron transport of charge and heat along  $\mathbf{B}$ .

Let  $\rho_{n_s s'}(z, p_z)$  be the spin polarization density matrix (Paper I) of electrons for the case when the electron gas is slightly non-uniform along  $\mathbf{B}$ . Here  $s$  and  $s'$  are the spin variables (Sect. 2). In the linear regime, deviations from the equilibrium are small. The zero-order density matrix is  $f(\varepsilon)\delta_{ss'}$ , where  $f(\varepsilon)$  is a local Fermi–Dirac distribution (2) which depends on  $z$  parametrically through  $\mu$  and  $T$ . In the first approximation, according to Paper I,

$$\begin{aligned} \rho_{n_s s'}(z, p_z) &= f(\varepsilon)\delta_{ss'} + \eta l \frac{\partial f(\varepsilon)}{\partial \varepsilon} \left[ e\mathcal{E} + \frac{\partial\mu}{\partial z} + \right. \\ &\quad \left. \frac{\varepsilon - \mu}{T} \frac{\partial T}{\partial z} \right] \varphi_{\eta n_s s'}(\varepsilon), \end{aligned} \quad (20)$$

where  $\eta = \text{sign}(p_z)$ , and the functions  $\varphi_{\eta n_s s'}(\varepsilon)$  determine non-equilibrium corrections to the density matrix;  $l$  is an electron scattering length:

$$\begin{aligned} l_{\text{ion}} &= \frac{m c^2 \hbar \omega_B}{2\pi n_i Z^2 e^4}, \quad l_{\text{ph}} = \frac{3}{4\pi n_i} \left( \frac{\hbar c}{Z e^2 r_{T1}} \right)^2, \\ l_{\text{imp}} &= \frac{m c^2 \hbar \omega_B}{2\pi n_{\text{imp}} (Z_{\text{imp}} - Z)^2 e^4}, \end{aligned} \quad (21)$$

$n_{\text{imp}}$  being the number density of impurities. The set of equations for  $\varphi_{\eta n s s'}(\varepsilon)$  has been derived in Paper I. Paper I presents also the mathematical formalism for solving these equations. After introducing the scale lengths (21), the equations describing the scattering on ions and impurities appear to be formally the same, i.e., there is no need to consider these scatterings separately. We shall refer to the scattering on ions and impurities as the *Coulomb (C)* scattering. If the functions  $\varphi_{\eta n s s'}(\varepsilon)$  are found, the transport coefficients in Eqs. (17) can be calculated as (Paper I)

$$\begin{pmatrix} \sigma \\ \beta \\ \lambda \end{pmatrix} = \frac{2m\omega_B l}{(2\pi\hbar)^2} \int_{mc^2}^{\infty} \begin{pmatrix} e^2 \\ e(\varepsilon - \mu)/T \\ (\varepsilon - \mu)^2/T \end{pmatrix} \times \Phi(\varepsilon) \left( -\frac{\partial f}{\partial \varepsilon} \right) d\varepsilon, \quad (22)$$

where

$$\Phi(\varepsilon) = \frac{1}{2} \sum_{\eta=\pm 1} \sum_{n=0}^{n(E)} \sum_{s=\pm 1} \varphi_{\eta n s s}(\varepsilon). \quad (23)$$

It is also convenient to introduce the function  $\Psi(E)$ ,

$$\Psi_C(E) = b^2 \Phi_C(\varepsilon), \quad \Psi_{\text{ph}}(E) = b \Phi_{\text{ph}}(\varepsilon). \quad (24)$$

Equations (22) can be written in a more transparent form if we introduce the effective energy dependent electron relaxation time:

$$\tau(\varepsilon) = \frac{el m \omega_B}{2(\pi \hbar c)^2 \mathcal{N}_e(\varepsilon)} \Phi(\varepsilon), \quad (25)$$

where  $\mathcal{N}_e$  is given by Eq. (6). Then

$$\begin{pmatrix} \sigma \\ \beta \\ \lambda \end{pmatrix} = \int_{mc^2}^{\infty} \begin{pmatrix} e^2 \\ e(\varepsilon - \mu)/T \\ (\varepsilon - \mu)^2/T \end{pmatrix} \times \frac{\mathcal{N}_e(\varepsilon) \tau(\varepsilon) c^2}{\varepsilon} \left( -\frac{\partial f}{\partial \varepsilon} \right) d\varepsilon, \quad (26)$$

where the energy integration represents the statistical averaging of the relaxation time with the energy derivative of the Fermi-Dirac distribution. Note that Eqs. (22) and (26) are valid for any electron degeneracy. Note also that Eqs. (19) and (41) of Paper I should contain  $\mathcal{N}_e(\varepsilon)$  instead of  $n_e$ .

Generally,  $\tau(\varepsilon)$  is an oscillating function of electron energy as discussed in Sect. 4. Let us mention one important case when  $\tau(\varepsilon)$  and  $\mathcal{N}_e(\varepsilon)$  vary with  $\varepsilon$  much slower than  $\partial f(\varepsilon)/\partial \varepsilon$ . Then, for strongly degenerate electrons, one obtains the results which look formally similar to those for  $B = 0$ :

$$\sigma \approx \frac{e^2 c^2 n_e \tau(\mu)}{\mu}, \quad \kappa \approx \lambda \approx \frac{\pi^2 k_B^2 T}{3e^2} \sigma, \quad \alpha \approx \frac{\pi^2 k_B^2 T}{3e} \frac{\partial}{\partial \varepsilon} \ln \left( \frac{\mathcal{N}_e(\varepsilon) \tau(\varepsilon)}{\varepsilon} \right) \Big|_{\varepsilon=\mu}, \quad (27)$$

with  $n_e = \mathcal{N}_e(\mu)$ .

The equations of this section are equally valid for the quantizing and non-quantizing magnetic fields.

## 4. Relaxation time $\tau(\varepsilon)$ (or $\Psi(E)$ )

### 4.1. Quantum oscillations

Evaluation of the transport coefficients  $\sigma$ ,  $\alpha$ , and  $\kappa$  consists of two stages. First, the equations of Paper I for  $\varphi_{\eta n s s'}(\varepsilon)$  should be solved and the function  $\Phi(\varepsilon)$  (or, equivalently,  $\Psi(E)$ , or  $\tau(\varepsilon)$ ) determined. Second, the energy integrations (22) have to be performed, and the transport coefficients (19) found. The second stage corresponds actually to the energy averaging of the relaxation time; it will be analysed in Sect. 5. Here we consider the first stage.

The main problem is to reproduce correctly *quantum oscillations* of  $\Psi(E)$  or  $\tau(\varepsilon)$  which occur since electrons of energy  $\varepsilon$  populate new Landau levels with growing  $\varepsilon$ . Population of an  $n$ -th level takes place when the energy variable  $\nu$  given by Eq. (7) exceeds  $n$ . The oscillations originate from the square root singularities of the density of states of free electrons in a magnetic field. Just behind the threshold for a given level ( $0 < (\nu - n) \ll 1$ )  $\Phi(\varepsilon)$  and  $\tau(\varepsilon)$  behave as  $\sqrt{\nu - n}$  which makes the oscillations important especially for not too high  $n$ .

Below we obtain practical equations for  $\Psi(E)$  or  $\tau(\varepsilon)$  at various electron energies.

### 4.2. Semiclassical approach for $\nu \gg 1$

If  $\nu \gg 1$  (electrons occupy many Landau levels),  $\Psi(E)$  can be calculated numerically, using the technique of Paper I, but it cannot be expressed in a closed analytic form. We will derive (Sect. 4.4) accurate fitting expressions based on the semiclassical approach described below.

When many Landau levels are occupied, the relaxation time  $\tau(\varepsilon)$  is expected to be close to the familiar classical non-magnetic quantity

$$\tau^{-1}(\varepsilon) = n_i v_0 \sigma_{\text{tr}}(\varepsilon), \quad (28)$$

where  $v_0$  is the electron velocity without magnetic quantization effects ( $v_0 = p_0 c^2 / \varepsilon$ ,  $p_0 = mc P_0 = mc \sqrt{E^2 - 1}$ ),  $n_i$  is the number density of scatterers, and  $\sigma_{\text{tr}}(\varepsilon)$  is the transport scattering cross section:

$$\sigma_{\text{tr}}(\varepsilon) = \int \frac{d\Omega}{4\pi} \int d\Omega' \sigma(\Theta) (1 - \cos \Theta). \quad (29)$$

In this case  $\sigma(\Theta)$  is the differential scattering cross section,  $\Theta$  is the scattering angle,  $d\Omega$  and  $d\Omega'$  are the solid angle elements of non-quantized electron momenta  $\mathbf{p}$  and  $\mathbf{p}'$  before and after scattering, respectively. In the Born approximation,

$$\sigma(\Theta) = \frac{|U(\mathbf{q})|^2 \varepsilon^2}{4\pi^2 \hbar^4 c^4} \left( 1 - \frac{v_0^2}{c^2} \sin^2 \frac{\Theta}{2} \right). \quad (30)$$

Assuming the isotropic distribution over momentum transfers  $\hbar \mathbf{q} = \mathbf{p}' - \mathbf{p}$  in the non-magnetic case, Eq. (29) can be rewritten as

$$\sigma_{\text{tr}}(\varepsilon) = \int \frac{d\Omega d\Omega'}{4\pi} \sigma(\Theta) \frac{3\hbar^2 q_z^2}{2p_0^2}. \quad (31)$$

Now consider weakly quantizing magnetic fields. Using Eq. (4), we can introduce the quantized transverse momentum  $p_{\perp}(n) = p_0 \sin \vartheta = \sqrt{2m\hbar\omega_B n}$ , where  $n$  is a Landau number, and  $\vartheta$  is an electron pitch angle. Accordingly, every  $n$  corresponds to two values of  $\vartheta$ , below and above  $\pi/2$ . Then an integration over  $\vartheta$  from 0 to  $\pi$  can be replaced as:

$$\int_0^{\pi} d\vartheta \sin \vartheta \dots \rightarrow \frac{m\hbar\omega_B}{p_0|p_z|} \sum_{n=0}^{n(E)} \sum_{\eta=\pm 1} \dots \quad (32)$$

At this stage we replace the integrals over  $\vartheta$  and  $\vartheta'$  in Eq. (31) by the sums over  $n$ ,  $\eta$  and  $n'$ ,  $\eta'$ . The dips of  $\tau(\varepsilon)$  or  $\Phi(\varepsilon)$  behind every Landau threshold are caused by the density-of-state singularity when either  $n$  or  $n'$  equals  $n(E)$ . Since  $n(E)$  is assumed to be large, these terms correspond to  $\vartheta \approx \pi/2$  or  $\vartheta' \approx \pi/2$ , respectively. The sum over  $\eta$  or  $\eta'$  in these terms is equivalent to introducing a factor 2. Thus, the term  $n = n(E)$  can be evaluated by setting  $\vartheta = \pi/2$  in Eq. (31), multiplying by  $2m\hbar\omega_B/(p_0|p_z|)$  and integrating over all remaining variables. The term  $n' = n(E)$  is similar. Then

$$\sigma_{\text{tr}}(\varepsilon) = \sigma_{\text{cl}}(\varepsilon) + \frac{3m\hbar\omega_B}{p_0|p_z|} \sigma_{\text{q}}(\varepsilon), \quad (33)$$

where

$$\sigma_{\text{cl}}(\varepsilon) = \int d\Omega' \sigma(\Theta) (1 - \cos \Theta), \quad (34)$$

$$\sigma_{\text{q}}(\varepsilon) = \int d\Omega' \sigma(\Theta) \cos^2 \vartheta' = \int d\Omega' \sigma(\Theta) \frac{\sin^2 \Theta}{2}. \quad (35)$$

The last term in Eq. (33) comes from the terms  $n = n(E)$ ,  $n' = n(E)$ . Its denominator contains the longitudinal momentum  $p_z$  at  $n = n(E)$  which vanishes just at a new Landau threshold and produces the required quantum oscillations. The first term,  $\sigma_{\text{cl}}(\varepsilon)$ , is non-oscillating. Actually it should be somewhat lower since we have subtracted the oscillating term from  $\sigma_{\text{tr}}$  but we neglect this difference in the present section. Equation (33) can also be inaccurate for small momenta transfers associated with the transitions between discrete neighboring  $n$  and  $n'$  (which require a more detailed consideration). In order to allow for this effect, we introduce the lower momentum transfer cutoff  $q = q_{\text{min}}$  while calculating  $\sigma_{\text{cl}}(\varepsilon)$  and  $\sigma_{\text{q}}(\varepsilon)$ . We specify  $q_{\text{min}}$  in Sect. 4.4.

From Eq. (13), for the scattering on ions we obtain

$$\sigma_{\text{cl,q}}^{\text{ion}}(\varepsilon) = 4\pi \left( \frac{Ze^2}{p_0 v_0} \right)^2 R_{\text{cl,q}}^{\text{C}}(E, y), \quad (36)$$

where

$$R_{\text{cl}}^{\text{C}}(E, y) = \Lambda_1 - \frac{v_0^2}{c^2} \Lambda_2,$$

$$R_{\text{q}}^{\text{C}}(E, y) = R_{\text{cl}}^{\text{C}}(E, y) - \Lambda_2 + \frac{v_0^2}{c^2} \Lambda_3,$$

$$\Lambda_k \equiv \frac{1}{2} \int_y^1 \frac{z^k dz}{(z+u)^2},$$

$$\begin{aligned} \Lambda_1 &= \frac{1}{2} \ln \left( \frac{1+u}{y+u} \right) - \frac{u(1-y)}{2(1+u)(y+u)}, \\ \Lambda_2 &= \frac{1-y}{2} - u \ln \left( \frac{1+u}{y+u} \right) + \frac{u^2(1-y)}{2(1+u)(y+u)}, \\ \Lambda_3 &= \frac{1-y^2}{4} - u(1-y) \\ &\quad + \frac{3}{2} u^2 \ln \left( \frac{1+u}{y+u} \right) - \frac{u^3(1-y)}{2(1+u)(y+u)}, \end{aligned} \quad (37)$$

$u = [\hbar q_s / (2p_0)]^2$  is the screening parameter, and  $y = [\hbar q_{\text{min}} / (2p_0)]^2$ .

For the scattering on impurities,  $\sigma_{\text{cl}}^{\text{imp}}(\varepsilon)$  and  $\sigma_{\text{q}}^{\text{imp}}(\varepsilon)$  are obtained from Eq. (36) by replacing  $Z \rightarrow (Z_{\text{imp}} - Z)$ .

In the case of the scattering on phonons, from Eqs. (15) and (33) we obtain

$$\sigma_{\text{cl,q}}^{\text{ph}}(\varepsilon, y) = \frac{8\pi}{3} \left( \frac{Ze^2}{\hbar v_0} \right)^2 r_{T1}^2 R_{\text{cl,q}}^{\text{ph}}(E, y), \quad (38)$$

where

$$R_{\text{cl}}^{\text{ph}}(E, y) = L_1 - L_2 \frac{v_0^2}{2c^2},$$

$$R_{\text{q}}^{\text{ph}}(E, y) = R_{\text{cl}}^{\text{ph}}(E, y) - \frac{1}{2} L_2 + \frac{v_0^2}{3c^2} L_3,$$

$$L_k = k \int_y^1 z^{k-1} e^{-wy} dy,$$

$$L_1 = \frac{1}{w} (e^{-wy} - e^{-w}),$$

$$L_2 = \frac{2}{w^2} [(1+wy)e^{-wy} - (1+w)e^{-w}],$$

$$L_3 = \frac{3}{w^3} [(2+2wy+w^2y^2)e^{-wy} - (2+2w+w^2)e^{-w}], \quad (39)$$

$w = (4/3)(p_0 r_{T2} / \hbar)^2$ . As explained in Sect. 3.1, these equations are strictly valid at  $T_{\text{D}} \lesssim T < T_{\text{m}}$ , and produce reasonable estimates at  $T_{\text{U}} \lesssim T \ll T_{\text{D}}$ .

Now, using Eqs. (28) and (33), we can easily express the inverse energy dependent relaxation time as a sum of the main (non-oscillating) and oscillating terms.

#### 4.3. Non-magnetic case

If  $B = 0$  the relaxation time of an electron is readily obtained from Eqs. (28), (33) by omitting the oscillating term and setting  $q_{\text{min}} = 0$  ( $y = 0$ ). Then we immediately recover Eqs. (23) – (28) of Paper I for  $\tau(\varepsilon)$  due to the Coulomb and phonon scatterings.

The function  $\Psi(E)$  is defined by Eq. (24). The function  $\mathcal{N}_e(\varepsilon)$  which enters Eq. (25) and relates  $\tau(\varepsilon)$  and  $\Psi(E)$  is given by Eq. (6). If  $B \rightarrow 0$ ,  $\mathcal{N}_e(\varepsilon)$  is easily calculated by replacing the sum over  $n$  with the integral, which yields the trivial result  $\mathcal{N}_e(\varepsilon) = (p_0/\hbar)^3 / (3\pi^2)$ . The appropriate functions  $\Psi(E)$  are

$$\Psi_{\text{C}}(E) = \frac{P_0^6}{3\Lambda(E)E^2}, \quad \Psi_{\text{ph}}(E) = \frac{P_0^4}{3E^2 R_{\text{cl}}^{\text{ph}}(E, 0)}, \quad (40)$$

where  $\Lambda(E) = R_{cl}^C(E, 0)$  is the Coulomb logarithm given by Eq. (24) of Paper I.

Once the energy dependent relaxation time  $\tau_0(\varepsilon)$  is known, the transport properties are easily evaluated from Eq. (27). In this way we reproduce familiar transport coefficients of degenerate electrons for the scattering mechanisms of study.

#### 4.4. Fitting expressions for $\nu > 1$

We have performed extensive calculations of  $\Psi(E)$  for the Coulomb and phonon scattering potentials, using the formalism of Paper I. We have mainly used the distribution function framework with the fixed-spin basis. According to Paper I, this yields sufficient accuracy in most cases of interest. However, the accuracy has been additionally controlled using the density matrix formalism. We have considered a wide range of magnetic fields  $10^{10} \text{ G} \lesssim B \lesssim 10^{14} \text{ G}$  sufficient for applications. In the case of the Coulomb potential,  $\Psi_C(E)$  depends also on the screening wavenumber  $q_s$  (Sect. 3.1). Instead of  $q_s$ , it is convenient to introduce the dimensionless screening parameter  $u = [\hbar q_s / (2p_0)]^2$ , defined in Eq. (37). We have calculated  $\Psi_C(E)$  treating  $u$  as a free parameter varied from 0 to 1. These results are equally valid for the scattering on ions and impurities (Sect. 3). In the case of the scattering on phonons,  $\Psi_{ph}(E)$  depends on the Debye–Waller factor defined in Eq. (15). The effect of this factor is described by the dimensionless parameter  $w = (4/3)(p_0 r_{T2} / \hbar)^2$  in accordance with Eq. (39). While calculating  $\Psi_{ph}(E)$ , we treat  $w$  as a free parameter varied in a wide interval,  $0 \leq w \lesssim 10$ .

Our computations cover an extended range of electron energies. The energy variable  $\nu$  has been varied up to 100, allowing population of up to 100 Landau energy levels.

We have produced vast tables of  $\Psi(E)$  (for different  $E$ ,  $b$ ,  $u$ ,  $w$ ). They are inconvenient for practical use but we have been able to fit all the results by analytic formulae. We have started with simple semiclassical Eqs. (28) and (33). They reproduce the main features of  $\Psi(E)$  at large  $\nu$  but they appear to be inexact near the Landau thresholds. We have managed to modify Eqs. (28) and (33) in such a way that the resulting formulae fit  $\Psi(E)$  accurately for any parameters  $b$ ,  $u$ ,  $w$  and for  $\nu > 1$ . We have treated the minimum momentum cutoff  $q_{min}$ , or  $y$  (Sect. 4.2), as a fit parameter. The fit formula reads ( $\nu > 1$ )

$$\Psi(E) = \sqrt{\Psi_a^2(E) + \Psi_b^2(E)}, \quad (41)$$

$$\Psi_a(E) = \Psi_0(E) \left[ R_{cl}(E, y) + \frac{3}{P_0} \left( \frac{b}{P_n} - b^{1/4} \sqrt{2P_n} \right) R_q(E, y) \right]^{-1}, \quad (42)$$

$$\Psi_0^C(E) = \frac{P_0^6}{3E^2}, \quad \Psi_0^{ph}(E) = \frac{P_0^4}{3E^2}, \quad (43)$$

where  $y = 0.5(P_n/P_0)^2$ ,  $P_n = \sqrt{E^2 - 1 - 2bn}$ ,  $n = n(E) = \text{Int}(\nu)$  in accordance with Eq. (7); the functions  $R_{cl}(E, y)$ ,  $R_q(E, y)$  are defined in Eqs. (37) and (39).

The expression for  $\Psi_b(E)$  depends on  $n$ . When  $n \geq 3$ , for all scattering mechanisms of study we have

$$\Psi_b(E) = \frac{P_0 P_n \Psi_0(E) / (3b)}{[R_q(E, y_+) + R_q(E, y_-)] (1 + \nu(P_n / \sqrt{b})^{5/2})}, \quad (44)$$

where  $y_{\pm} = 0.5[(P_{n-1} \pm P_n) / P_0]^2$ . When  $n = 1$  or 2, we obtain

$$\Psi_b(E) = \frac{P_0 P_n}{Q_2(\xi_+ + \xi_s, 0, 1) + Q_2(\xi_- + \xi_s, 0, 1)} \times \frac{1}{[(E+1)/2]^2 + [b/(E+1)]^2}, \quad (45)$$

where  $\xi_{\pm} = (P_0 \pm P_n)^2 / (2b)$ ,  $\xi_s^C = (a_m q_s)^2 / 2$ ,  $\xi_s^{ph} = 0$ , and  $a_m = \sqrt{\hbar c / (eB)}$  is the magnetic quantum length. The functions  $Q_2(\xi, n', n)$  have been introduced in Paper I. We have

$$Q_2^C(\xi, 0, 1) = \int_0^{\infty} \frac{\zeta e^{-\zeta}}{(\zeta + \xi)^2} d\zeta = (1 + \xi) e^{\xi} E_1(\xi) - 1, \\ Q_2^{ph}(\xi, 0, 1) = \int_0^{\infty} \frac{\zeta e^{-\zeta g - g\xi + \xi}}{\zeta + \xi} d\zeta \\ = \frac{e^{-g\xi + \xi}}{g} [1 - g\xi e^{g\xi} E_1(g\xi)], \quad (46)$$

where  $g = 1 + w / (4\nu)$ , and  $E_1(\xi)$  is the integral exponent which is easily calculated (Abramowitz & Stegun 1972).

Equations (41)–(42) are valid for the Coulomb and phonon scatterings. The function  $\Psi_a(E)$  is associated with the modified semiclassical expression of  $\Psi(E)$  (Sect. 4.2), whereas  $\Psi_b(E)$  is introduced to improve the fit accuracy just behind a new Landau level threshold, at  $(\nu - n) \ll 1$ . In the limit of  $B \rightarrow 0$  the equations reproduce the correct non-magnetic expression  $\Psi(E) = \Psi_0(E) / R_{cl}(E, 0)$ .

The fitting equations describe the tables of  $\Psi(E)$  for all values of  $b$ ,  $u$ ,  $w$  (see above) at any energy  $E$ . They are based on the correct semiclassical expressions (Sect. 4.2), and their accuracy does not become worse with increasing  $E$  as demonstrated in Figs. 2 and 3. The figures present  $\Phi(E)$  versus  $\nu$  for different scattering mechanisms, magnetic fields  $b$ , and charge numbers  $Z$ . For illustration, the screening wavenumber  $q_s$  in the case of the Coulomb scattering has been calculated assuming strong degeneracy, with the Fermi level being equal to the current value of electron energy,  $\mu = \varepsilon$ . This allows us to find the electron number density from Eq. (5), and determine then  $q_s$  from Eqs. (13) and (14). For the scattering on phonons, we have considered several values of  $T$  which enter the Debye–Waller factor defined in Eq. (15). If  $T_7 \ll 1$ , the Debye–Waller factor is negligible, i.e.,  $e^{-2W} = 1$  in Eq. (15). Fig. 2 demonstrates population of the low-lying Landau levels  $n=1, 2, 3$  and 4. Fig. 3 displays population of higher levels,  $n = 20$  and  $n = 99$ . The overall accuracy of the fits is around 3% which seems to be satisfactory for fitting oscillating functions. The accuracy becomes worse (up to 8% for  $n > 5$ ) at  $0 < \nu - n \ll 1$ , where  $\Psi(E)$  contains dips, but this is not important: the dips are easily smeared out due to subsequent energy averaging of  $\Psi(E)$  (Sect. 5).

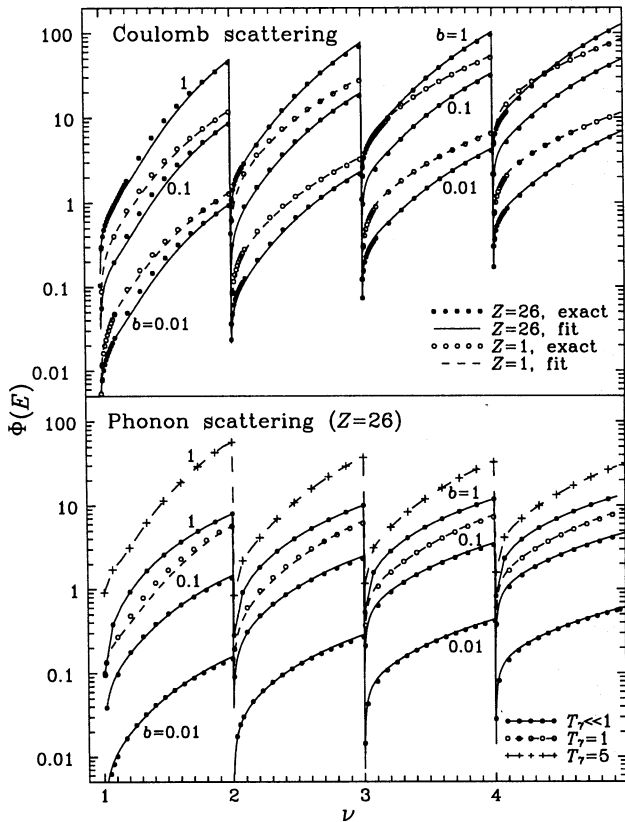


**Fig. 2.** Calculated and fitted function  $\Phi(E)$  versus  $\nu$  for Coulomb and phonon scatterings at different parameters of matter in the case when the electrons populate the Landau levels  $n=1,2,3,4$ .

Previously the function  $\Phi(E)$  was calculated and fitted, accurately and thoroughly, by Hernquist (1984). The author considered the Coulomb and high- $T$  phonon scatterings in iron matter at  $B = 10^{10}, 3 \times 10^{10}, 10^{11}, 3 \times 10^{11}, 10^{12}, 3 \times 10^{12}, 10^{13}, 3 \times 10^{13}, 10^{14}$  G and included population of  $n < 30$  Landau levels. His fit formula (his Eq. (178)) contained 3 adjustable parameters for every Landau level (90 fit parameters for every  $B$  and each scattering mechanism). However, Hernquist (1994) did not take into account the Debye–Waller factor which made his results for the phonon scattering not very accurate (Paper I). Our fitting formulae require no tables of fit parameters; they are valid for any magnetic field and Landau level number of practical interest, as well as for any chemical element.

#### 4.5. Low energies, $\nu < 1$

If  $\nu < 1$ , the electrons with energy  $\varepsilon$  occupy the ground Landau level  $n=0$ . In this case  $\Psi(E)$  is expressed in a closed form using the results of Paper I. For the Coulomb and phonon scatterings, we obtain

$$\Phi(E) = \frac{P_0^2 b^k}{2Q_2(\xi_+ + \xi_s, 0, 0)}, \quad (47)$$

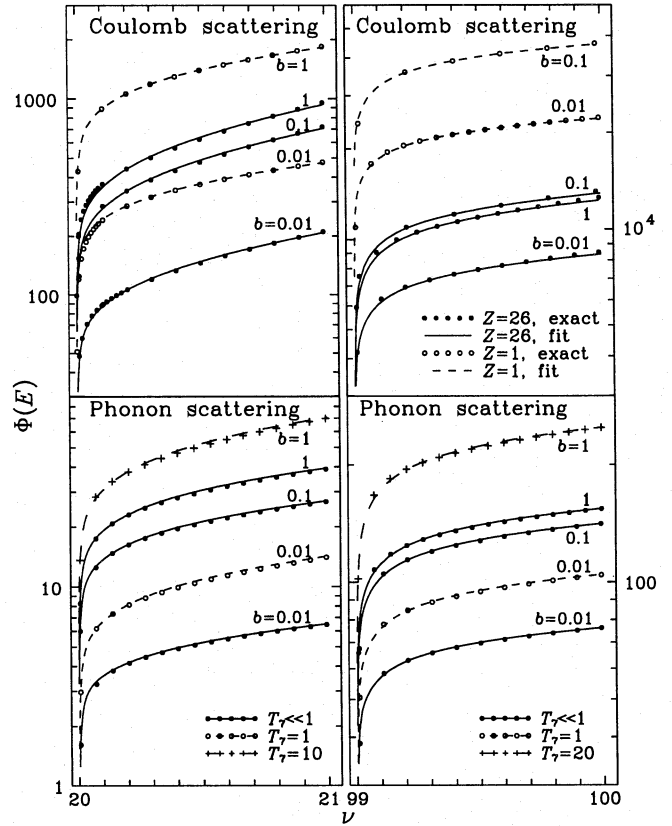


**Fig. 3.** Same as in Fig. 2 for population of the Landau levels  $n=20$  and  $99$ .

where  $k_C = 2$ ,  $k_{ph} = 1$ ,  $\xi_+ = 2P_0^2/b$ , and  $\xi_s$  is defined in (45). The function  $Q_2(\xi, 0, 0)$  is (cf. Eq. (46))

$$Q_2^C(\xi, 0, 0) = \int_0^\infty \frac{e^{-\zeta}}{(\zeta + \xi)^2} d\zeta = \frac{1}{\xi} - e^\xi E_1(\xi),$$

$$Q_2^{ph}(\xi, 0, 0) = \int_0^\infty \frac{e^{-\zeta g - g\xi + \xi}}{\zeta + \xi} d\zeta = e^\xi E_1(g\xi). \quad (48)$$

The electron transport properties in the ultra-quantum limit  $\nu \ll 1$  are discussed, for instance, by Yakovlev (1980, 1984).

### 5. Energy averaging of relaxation time or $\Psi(E)$

The results of Sects. 4.4 and 4.5 fully determine  $\Psi(E)$ . The next step is to evaluate the longitudinal electron transport coefficients from Eqs. (19) and (22). This should be done by a numerical energy integration in Eq. (22). The integration corresponds to statistical energy averaging of the relaxation time which broadens the quantum oscillations. The broadening is produced by the *thermal effects*: all electrons with energies  $|\varepsilon - \mu| \lesssim k_B T$  are known to contribute into the transport properties.

Actually, quantum oscillations can also be broadened by other mechanisms which have been neglected in Sect. 3 and 4 (since we have used the Born approximation and assumed strictly elastic electron scattering, see Paper I). Exact theory of the broadening would have been very sophisticated, and it is



still absent. We incorporate the effects of the broadening in an approximate manner. In addition to the thermal broadening, we will take into account the *collisional* broadening of the Landau levels, and the broadening due to weak *inelasticity* of electron collisions.

To include these effects we replace  $(\varepsilon - \mu)$  by  $(\varepsilon - \mu)T/T_k$  in the integrands of Eq. (22), with  $T_k = T + [(\gamma + \Delta\varepsilon)/(2\pi k_B)]$ . Here  $\gamma$  is the collisional width of the Landau energy levels which we set equal to  $\gamma = \hbar/\tau_0$ ,  $\tau_0$  being the field-free electron relaxation time (Sect. 4.3; Paper I). We include  $\gamma$  into  $T_k$  in a way familiar to the semi-quantitative treatment of magnetic oscillations in terrestrial metals (e.g., Shoenberg 1984). In solid matter,  $T < T_m$ , we set  $\gamma = \gamma_{\text{ph}} + \gamma_{\text{imp}}$  (even for  $T < T_U$ , ignoring the failure of our low- $T$  phonon treatment for very low  $T$ , Sect. 3.1). The quantity  $\Delta\varepsilon$  is a typical energy transfer of an electron in a collision event. We set  $(\Delta\varepsilon)_{\text{ion}} \approx \hbar\omega_p + v_i p_{F0}$ ,  $(\Delta\varepsilon)_{\text{ph}} \approx \hbar\omega_p G_0(t)$ , and  $(\Delta\varepsilon)_{\text{imp}} \approx 0$ , where  $\omega_p$  is the ion plasma frequency,  $v_i$  is the ion thermal velocity,  $G_0(t)$  (with  $t = T/T_p$ ) describes reduction of typical frequencies of phonons excited or absorbed by electrons at  $T \ll T_D$ . We set  $G_0(t) \sim G(t)$ , where  $G(t)$  is the reduction factor introduced in Sect. 3.1. Our choice of  $\gamma$  and  $\Delta\varepsilon$  is rather phenomenological. However the results (the transport coefficients) are not too sensitive to this choice. If more accurate values of  $\gamma$  and  $\Delta\varepsilon$  appear in the future, they could easily be incorporated in our calculation scheme.

Using Eqs. (19), (22), and (24), we obtain the following practical equations for the longitudinal electric conductivity  $\sigma$ , thermal conductivity  $\kappa$  and thermopower  $\alpha$  as functions of electron chemical potential  $\mu$ , temperature  $T$ , magnetic field  $B$ , and nuclear composition of matter:

$$\begin{aligned} \sigma &= I_0, \quad \kappa = \frac{\pi^2 k_B^2 T}{3e^2} J_\kappa, \quad \alpha = \frac{k_B}{e} J_\alpha, & (49) \\ J_\kappa &= I_2 - \frac{I_1^2}{I_0}, \quad J_\alpha = \frac{I_1}{I_0}, \\ I_j &= \frac{\sigma_0}{\theta} \int_1^\infty dE \Psi(E) \zeta^j \frac{e^\zeta}{(e^\zeta - 1)^2}, \\ \sigma_0^{\text{ion}} &= \frac{m^4 c^6}{4\pi^3 \hbar^3 e^2 n_i Z^2} \approx 2.473 \times 10^{22} \frac{A}{\rho_6 Z^2} \text{ s}^{-1}, \\ \sigma_0^{\text{imp}} &= \sigma_0^{\text{ion}} \frac{Z^2 n_i}{(Z_{\text{imp}} - Z)^2 n_{\text{imp}}}, \\ \sigma_0^{\text{ph}} &= \frac{m^2 c^4}{\hbar k_B T u_{-2}} \approx 1.794 \times 10^{21} \frac{1}{T_7} \text{ s}^{-1}. & (50) \end{aligned}$$

In this case  $\zeta = (\varepsilon - \mu)/(k_B T_k)$ , and  $\theta = k_B T_k/(mc^2)$ .

Equations (49) allow us to evaluate the required transport coefficients for any parameters of study indicated in Sect. 2 and 4.4.

The integration in  $I_j$  has been optimized taking into account oscillating behaviour of  $\Psi(E)$  and the square root singularities at the Landau thresholds  $E_n = \sqrt{1 + 2bn}$ . The integrals are presented as sums of separate integrals over all those intervals  $[E_n, E_{n+1}]$  which fall in range from  $E = E_\mu - 40\theta$  to  $E = E_\mu + 40\theta$ , with  $E_\mu = \mu/(mc^2)$ .

For high enough temperatures, when this range covers more than 25 thresholds of the Landau levels  $n$ , integration in  $I_j$  over every selected interval  $[E_n, E_{n+1}]$  is carried out using Eq. 25.4.34 of Abramowitz & Stegun (1972) with 4 mesh points between neighboring Landau thresholds. This procedure is specifically adopted for integrand functions which behave as  $\sqrt{E - E_n}$  in the vicinity of  $E = E_n$ .

For low temperatures, a more accurate numerical integration is required near  $E = E_\mu$ . For this purpose, we select those intervals  $[E_n, E_{n+1}]$  which span the range from  $E = E_\mu - 8\theta$  to  $E_\mu + 8\theta$ . One or two of the selected intervals which include the points  $E = E_\mu \pm 8\theta$  are further subdivided by these boundary points. We integrate over any such interval using the 128-point Simpson formula. The integration over intervals not spanning the selected range is done as in the case of high temperatures.

This algorithm ensures fast and accurate (with error  $\lesssim 0.1\%$ ) evaluation of the integrals  $I_j$ .

In order to combine the scattering on low-temperature phonons and impurities at low  $T$  we ignore the breakdown of the low- $T$  phonon approximation at  $T \sim T_U$ . We evaluate separately the integrals  $I_j$  ( $j=0, 1, 2$ ) in Eqs. (50) due to the phonon and impurity scatterings at  $T < T_m$ . Then we calculate the total values of  $I_j$  for  $T < T_m$  as  $I_j^{-1} = (I_j^{\text{ph}})^{-1} + (I_j^{\text{imp}})^{-1}$ , and determine the transport coefficients from Eqs. (49) and (50).

For practical purpose, we should also calculate the electron number density  $n_e$  (which specifies mass density  $\rho = m_u n_e(A/Z)$ ) and its derivative with respect to the chemical potential that determines the electron screening wavenumber  $q_e$  according to Eq. (14). The practical expressions for  $n_e$  and  $\partial n_e/\partial \mu$  are given in Appendix C of Paper I. In these expressions we will also include the broadening of the Landau levels. The thermal broadening is naturally implanted in these equations just as in Eq. (22). The inelastic scattering can be important for the kinetic properties but is inadequate for thermodynamics. Thus, we incorporate the collisional broadening by replacing  $T \rightarrow T_{\text{th}} = T + [\gamma/(2\pi k_B)]$  in Eqs. (C1) and (C3) of Paper I.

In practice, one often needs the transport coefficients as a function of mass density  $\rho$  rather than the electron chemical potential  $\mu$ . The inverse dependence of  $\mu$  on  $\rho$  and  $T$  can be found by iterations from the fitting formula for  $n_e(\mu)$  given in Paper I. For example, if the electrons populate several Landau levels and  $\mu > mc^2$ , we use the following rapidly converging algorithm. The zero-order value of  $\mu$  can be set equal to  $\mu_0 = c\sqrt{(mc)^2 + p_{F0}^2}$ , the field-free value (3) in the limit of strong degeneracy. At any subsequent iteration step  $i = 1, 2, 3, \dots$ , we calculate  $n_e^{(i)}$  from the fitting formula with  $\mu = \mu_{i-1}$ . Then we determine  $\mu_i$  for the next iteration as  $\mu_i = c\sqrt{(mc)^2 + p_i^2}$ , taking  $p_0 = p_{F0}$  and  $p_i = p_{i-1}(n_e/n_e^{(i-1)})^{1/3}$ .

## 6. Results and discussion

Using the results of Sect. 4 and 5, we have created a computer code which calculates the longitudinal electric and thermal conductivities and the thermopower of degenerate electrons for densities  $10^4 \text{ g cm}^{-3} < \rho \lesssim 4 \times 10^{11} \text{ g cm}^{-3}$ , magnetic fields  $B \lesssim 10^{14} \text{ G}$ , and arbitrary nuclear composition in the outer

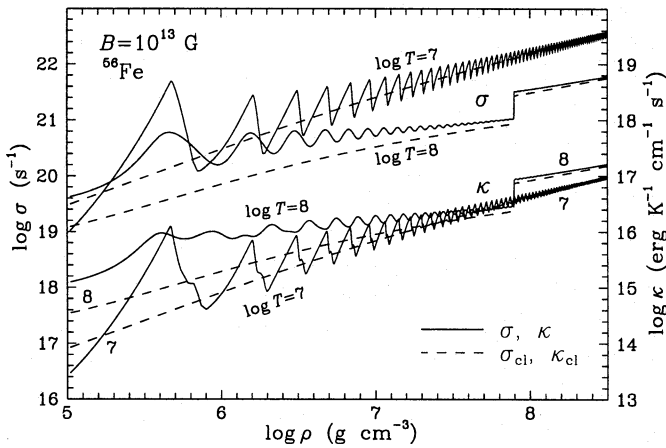


Fig. 4. Electric (left vertical scale, upper lines) and thermal (right scale, lower lines) conductivities of  $^{56}\text{Fe}$  matter vs density for  $B = 10^{13}$  G (solid lines) and  $B = 0$  (dashes) at  $T = 10^7$  K and  $10^8$  K.

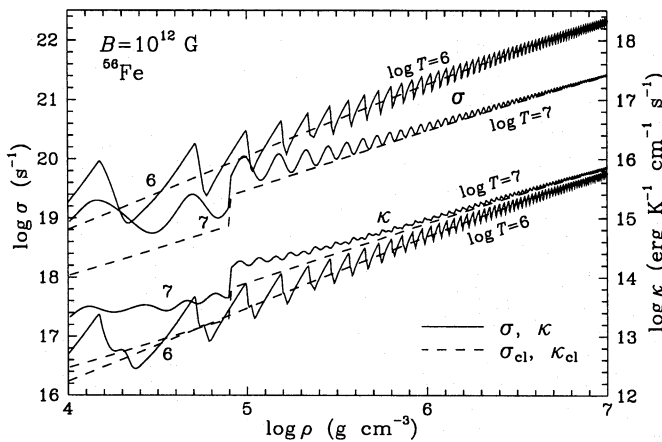


Fig. 5. Same as in Fig. 4 for  $B = 10^{12}$  G at  $T = 10^6$  and  $10^7$  K.

crust of a neutron star (as described in Sects. 2, 3.1, and 4.4). The code is based on theoretical formalism that is strictly justified for the Coulomb scattering of electrons on ions at  $T > T_m$ , for the scattering on high-temperature phonons at  $T_D \lesssim T \lesssim T_m$ , and for the scattering on impurities at  $T < T_m$ . The results are also valid (semi-quantitatively) for the low-temperature phonon scattering at  $T_U \lesssim T \ll T_D$  as discussed in Sect. 3.1.

Figs. 4 – 8 show typical density dependence of the longitudinal transport coefficients in a neutron star crust with a strong magnetic field.

Fig. 4 demonstrates quantum oscillations of the electric and thermal conductivities with increasing density in  $^{56}\text{Fe}$  matter for  $B = 10^{13}$  G at two temperatures,  $T = 10^7$  K and  $10^8$  K. Every oscillation is associated with population of a new Landau level, starting from the first excited level  $n = 1$  at  $\rho \approx \rho_B \approx 5 \times 10^5$  g cm $^{-3}$  (cf. Fig. 1). In the displayed density range ( $10^5$  g cm $^{-3} < \rho < 3 \times 10^8$  g cm $^{-3}$ ), up to about 60 Landau levels are populated. For comparison, dashed lines show the conductivities  $\sigma_{cl}$  and  $\kappa_{cl}$  in the absence of the magnetic field.

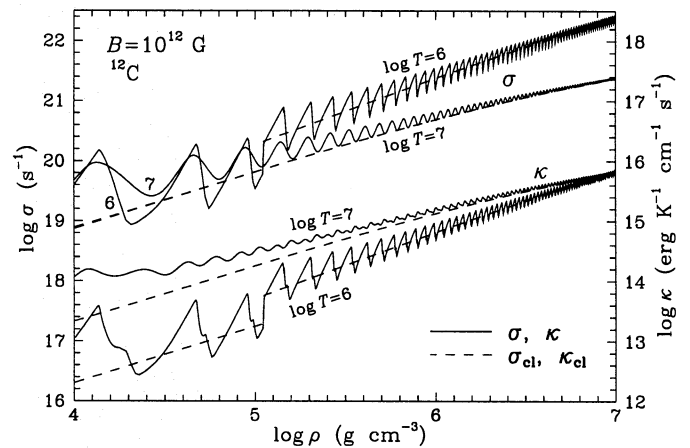


Fig. 6. Same as in Fig. 5 for  $^{12}\text{C}$  matter.

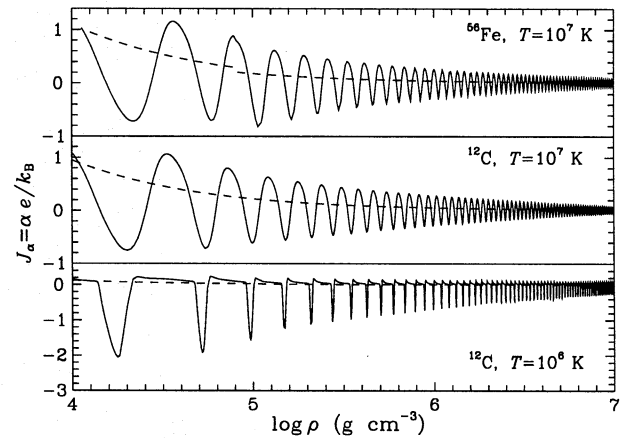
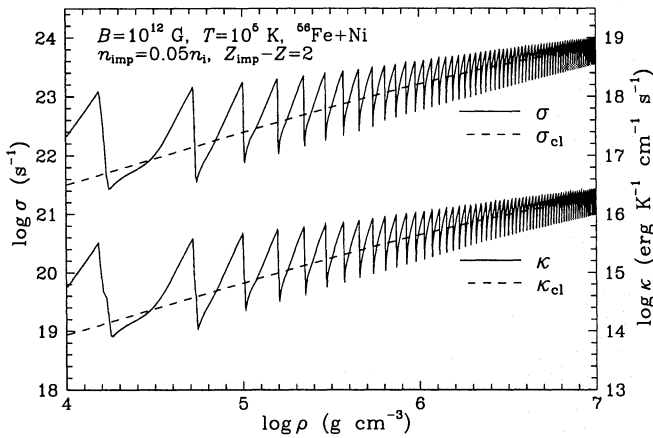


Fig. 7. Dimensionless longitudinal thermopower for  $^{56}\text{Fe}$  and  $^{12}\text{C}$  matter,  $B = 10^{12}$  G and  $T = 10^6$  and  $10^7$  K. Dashes show the  $B = 0$  curves.

For the lower temperature,  $T = 10^7$  we have  $T \ll T_B$  (see Fig. 1). The adopted magnetic field  $B = 10^{13}$  G is quantizing (Sect. 2), and the oscillations are quite pronounced. At this temperature, matter is solid ( $T < T_m$ ), and the oscillations are produced by the scattering of electrons on phonons. These oscillations are significantly amplified by the Debye–Waller suppression of the electron scattering (Paper I). In the domain of strongly quantizing magnetic field ( $\rho \lesssim \rho_B$ , Sect. 2), the transport coefficients differ drastically from those at  $B = 0$ . With increasing  $\rho$  in the domain of weakly quantizing fields ( $\rho \gg \rho_B$ ,  $T \ll T_B$ ), the oscillations become weaker, and the conductivities are seen to be close to the non-magnetic ones. Every oscillation of the electric conductivity contains one maximum and subsequent dip, while the oscillation of the thermal conductivity may show a secondary maximum as explained, for instance, by Yakovlev (1980, 1984). The amplitudes of quantum oscillations of the electron conductivity are always stronger than those of the thermal conductivity.

For the higher temperature  $T = 10^8$  K in Fig. 4, the magnetic field  $B = 10^{13}$  G is less quantizing (the ratio  $T_B/T$  remains



**Fig. 8.** Same as in Figs. 4–6 for electron scattering on charged impurities in  $^{56}\text{Fe}$  matter at  $B = 10^{12}$  G.

larger than unity but it is 10 times smaller than for  $T = 10^7$  K). Accordingly, the quantum oscillations are noticeably weaker due to the thermal broadening of the Landau levels. The broadening is more pronounced in the thermal conductivity than in the electric conductivity. The jumps of the transport coefficients at  $\rho \approx 10^8$  g cm $^{-3}$  are associated with solidification. For lower  $\rho$  (at given  $T$ ), matter is melted, and the electron relaxation is produced by the Coulomb scattering on ions. For higher  $\rho$ , ions solidify, and the electrons scatter on phonons just as at  $T = 10^7$  K. At higher  $T \sim T_B$ , the oscillations would be entirely smeared out by the thermal broadening. Note that the transport coefficients in the ion liquid with the magnetic field at  $T = 10^8$  K are systematically larger than those in the non-magnetic matter. This means that the transport coefficients averaged over magnetic oscillations are larger than the coefficients for  $B = 0$ . This difference between the oscillation-averaged and non-magnetic coefficients is explained by the classical effect of the electron Larmor rotation on the Coulomb logarithm in the transport cross section for the electron–ion scattering: the non-quantizing magnetic field decreases the Coulomb logarithm (and amplifies the electric and thermal conductivities) by reducing the maximum effective impact parameter (e.g., Yakovlev 1980).

Fig. 5 shows quantum oscillations of the transport coefficients in iron matter with weaker magnetic field,  $B = 10^{12}$  G, at lower  $T$  ( $10^6$  and  $10^7$  K). Since the magnetic field is lower, the oscillations associated with population of the same Landau levels occur at lower  $\rho$  (cf. Fig. 1). If  $T = 10^6$  K, matter is solid in the displayed density range,  $10^4$  g cm $^{-3} < \rho < 10^7$  g cm $^{-3}$ , while for  $T = 10^7$  K it solidifies at  $\rho \approx 8 \times 10^4$  g cm $^{-3}$ . Qualitative behavior of the curves is the same as in Fig. 4.

Fig. 6 presents quantum oscillations of the thermal and electric conductivities in carbon matter for  $B = 10^{12}$  G at  $T = 10^6$  and  $10^7$  K. The main features are the same as in Figs. 4 and 5, although the melting temperature  $T_m$  ( $\Gamma = 172$ , Eq. (11)) is lower than for iron. Population of the Landau levels is mainly independent of ion species ( $A, Z$ ), and occurs at the same  $\rho$  as in Fig. 5. If  $T = 10^7$  K, matter is melted, in the displayed parameter range. In the case of  $T = 10^6$  K, matter is liquid for

$\rho \lesssim 10^5$  g cm $^{-3}$  and solid at higher  $\rho$ . In this case quantum oscillations are pronounced stronger than at  $T = 10^7$  K.

Fig. 7 shows quantum oscillations of the dimensionless longitudinal thermopower  $J_\alpha = \alpha e/k_B$  (defined by Eq. (49)) for  $B = 10^{12}$  G. The upper panel corresponds to iron matter at  $T = 10^7$  K (cf. Fig. 5). Two lower panels correspond to carbon matter for the same conditions as in Fig. 6. The thermopower is known to be more sensitive to the electron scattering mechanism, than the conductivities. Its quantum oscillations are seen to be stronger, and more complicated. The oscillating thermopower differs significantly from that at  $B = 0$ , and it can change sign (Yakovlev 1980, 1984). The jumps associated with the solidification are pronounced weaker than in the conductivities.

The curves displayed in Figs. 4–7 are calculated taking into account collisional and inelastic-scattering broadening of the Landau levels (Sect. 5). These broadening mechanisms appear to be less significant than the thermal broadenings for the scattering on ions in Coulomb liquid and on phonons in the crystalline matter. Nevertheless non-thermal broadenings become more important with decreasing temperature. In particular, the inelastic-scattering broadening becomes significant at  $T \ll T_D$ , when the employed approximation of high-temperature phonons breaks (Sect. 3.1). The collisional and inelastic-scattering broadenings also become important with decreasing density near the domain of incomplete ionization (Sect. 2).

Fig. 8 shows oscillations of the electric and thermal conductivities produced by electron scattering on charged impurities in iron matter with  $B = 10^{12}$  G at low temperature  $T = 10^5$  K assuming, for illustration, that the scattering on phonons is inefficient. The impurity number density is supposed to be  $n_{\text{imp}} = 0.05 n_i$ , and the impurity charge number is  $Z_{\text{imp}} = 28$ . The impurity screening wavenumber  $q_{\text{imp}}$  in Eq. (16) is set equal to  $q_{\text{imp}} = (4\pi n_{\text{imp}}/3)^{1/3}$ . At this low temperature, the collisional broadening of the Landau levels becomes more important. With decreasing  $T$ , the thermal broadening would die out, and the shapes of the oscillations would be entirely determined by the collisional broadening. Note that we include the non-thermal broadening mechanisms in an approximate manner. This introduces an uncertainty into the transport coefficients at low temperatures. However the case of low temperatures is not very important for applications. Anyway, the number density and charge number of impurities are not known, and this introduces much larger uncertainty in our knowledge of the transport properties of very cold stellar matter.

## 7. Summary

We have obtained practical formulae for evaluation of the longitudinal electric and thermal conductivities and longitudinal thermopower in degenerate dense matter ( $10^4$  g cm $^{-3} \lesssim \rho \lesssim 4 \times 10^{11}$  g cm $^{-3}$ ) of outer neutron star crusts with strong magnetic fields  $B = 10^{10} - 10^{14}$  G (at stronger fields, the splitting of electron Landau levels concerned with anomalous electron magnetic moment should be taken into account). The results are expressed in terms of the energy averaged electron relax-

ation time  $\tau(\varepsilon)$  or the function  $\Psi(E)$ . We have found (Sect. 4) accurate and simple analytic fits for  $\Psi(E)$ , which are valid in wide ranges of the parameters of stellar matter for three electron scattering mechanisms: for the Coulomb scattering on ions in gaseous or liquid phases, for the scattering on high-temperature phonons in solid matter, and for the scattering on charged impurities in solids at low temperatures. We have proposed (Sect. 5) an efficient energy averaging procedure which allows us to evaluate rapidly any longitudinal electron transport coefficient. The numerical examples are given in Sect. 6.

Note that our formalism can easily be extended to higher densities,  $\rho > 4 \times 10^{11} \text{ g cm}^{-3}$ , in the inner crust of a neutron star, where free neutrons appear in matter in addition to electrons and atomic nuclei. In this case nuclei can occupy substantial part of volume, and one should take into account finite sizes of nuclei by multiplying the Fourier image of the scattering potential,  $|U(\mathbf{q})|^2$  (Sect. 3.1), by a squared nuclear formfactor (e.g., Itoh et al. 1984). However, this effect can be shown to be not very strong. For instance, in the absence of the magnetic field, it reduces the effective electron collision frequencies typically by about 20 %, in the inner crusts of neutron stars. Accordingly, the present theoretical framework is expected to be sufficiently accurate in the inner crusts as well.

The results of this work are required for studying various processes in neutron star crusts (e.g., Yakovlev & Kaminker 1994). First of all, we mention thermal evolution (cooling) of neutron stars. The outer crust produces thermal isolation of the stellar interior. The electron thermal conductivity is most important for calculating the relationship between the surface and interior temperatures of the star and for evaluating the distribution of the temperature over the neutron star surface. The latter distribution can be strongly anisotropic owing to anisotropic character of the thermal conductivity. The anisotropy of the surface temperature leads to modulation of the surface thermal radiation due to stellar rotation. The modulation has been observed with *ROSAT* in soft X-ray radiation of several neutron stars, in particular, PSR 0656+14 (Finley et al. 1992, Anderson et al. 1993) and Geminga (Halpern & Holt 1992, Halpern & Ruderman 1993). Correct interpretation of observations requires the knowledge of the distribution of the effective temperature over the neutron star surface combined with the solution of the radiative transfer problem in the neutron star atmosphere (e.g., Pavlov et al. 1995). Much work has already been done by Hernquist (1984), Van Riper (1988, 1991) and Schaaf (1988, 1990) in calculating the temperature profiles in neutron star crusts with quantizing magnetic fields, and in analysing the cooling of magnetized neutron stars. Many important and reliable results concerning the temperature profiles have already been obtained (particularly, by Van Riper 1988) in the approximation of uniform plane-parallel layer with the magnetic field normal to the surface. However the overall problem of the surface temperature distribution is complicated and requires further study (as discussed, e.g., by Yakovlev & Kaminker 1994). The solution of this problem can be based, to some extent, on the above results. Secondly, the electric conductivity and thermopower are important for understanding the evolution of neutron star mag-

netic fields (e.g., Urpin et al. 1986, 1994). We plan to construct the models of outer crusts of neutron stars with strong magnetic fields in our subsequent works.

The Fortran computer code for evaluating the transport properties based on the above results is distributed freely by electronic mail upon request.

*Acknowledgements.* Useful discussions with C.J. Pethick and valuable comments of K.A. Van Riper are gratefully acknowledged. This work was supported in part by RBRF (grant 96-02-16870), ISF (grant R6A300), and INTAS (grant 94-3834). A.Y.P. is grateful to the Nordita staff and especially to C.J. Pethick for hospitality.

## References

- Abramowitz, M., Stegun, I.A. (eds.) 1972, Handbook of Mathematical Functions, Dover, New York
- Anderson, S.B., Córdoba, F.A., Pavlov, G.G., Robinson, C.R., Thompson, R.J. 1993, ApJ, 414, 867
- Baiko, D.A., Yakovlev, D.G. 1995, Astron. Lett., 21, 702
- Canuto, V., Ventura, J. 1977, Fundam. Cosmic Phys., 2, 203
- Carr, W.J. 1961, Phys. Rev., 122, 1437.
- Ceperley, D.M., Alder, B.J. 1980, Phys. Rev. Lett., 45, 566
- Finley, J.P., Ögelman, H., Kiziloğlu, Ü. 1992, ApJL, 394, L21
- Hansen, J.-P. 1973, Phys. Rev., A8, 3096
- Halpern, J.P., Holt, S.S. 1992, Nature, 357, 222
- Halpern, J.P., Ruderman, M. 1993, ApJ, 415, 286
- Hernquist, L. 1984, ApJS, 56, 325
- Itoh, N., Kohyama, Y., Matsumoto, N., Seki, M. 1984, ApJ, 285, 758; erratum 404, 418
- Itoh, N., Hayashi, H., Kohyama, Y. 1993, ApJ, 418, 405
- Landau, L.D., Lifshitz, E.M. 1976, Quantum Mechanics, Pergamon, Oxford
- Mochkovitch, R., Hansen, J.-P. 1979, Phys. Lett., A73, 35
- Nagara, H., Nagata, Y., Nakamura, T. 1987, Phys. Rev., A36, 1859
- Pavlov, G.G., Shibano, Yu.A., Zavlin, V.E., Meyer, R.D. 1995, in M.A. Alpar, Ü. Kiziloğlu, J. van Paradijs (eds.), The Lives of the Neutron Stars, Kluwer Academic Publishers, Dordrecht, p. 71
- Potekhin, A.Y. 1996, A&A, 306, 999 (Paper I)
- Raikh, M.E., Yakovlev, D.G. 1982, Ap&SS, 87, 193
- Rögnvaldsson, Ö.E., Fushiki, I., Gudmundsson, E.H., Pethick, C.J., Yngvason, J. 1993, ApJ, 416, 276
- Schaaf, M.E. 1988, A&A, 205, 335
- Schaaf, M.E. 1990, A&A, 235, 499
- Shoenberg, D. 1984, Magnetic oscillations in metals, Cambridge Univ. Press, Cambridge
- Urpin, V.A., Yakovlev, D.G. 1980, SvA, 24, 425
- Urpin, V.A., Levshakov, S.A., Yakovlev, D.G. 1986, MNRAS, 219, 703
- Urpin, V.A., Chanmugam, G., Sang, Y. 1994, ApJ, 433, 780
- Usov, N.A., Grebenshchikov, Yu.B., Ulinich, F.R. 1980, Zh. Eksper. Teor. Fiz. (Sov. Phys.-JETP), 78, 296
- Van Riper, K.A. 1988, ApJ, 329, 339
- Van Riper, K.A. 1991, ApJS, 75, 449
- Yakovlev, D.G. 1980, Preprint No. 678 Ioffe Phys.-Tech. Inst., Leningrad
- Yakovlev, D.G. 1984, Ap&SS, 98, 37
- Yakovlev, D.G., Kaminker, A.D. 1994, in G. Chabrier, E. Schatzman (eds.), The Equation of State in Astrophysics, Cambridge Univ. Press, Cambridge, p. 214
- Yakovlev, D.G., Urpin, V.A. 1980, SvA, 24, 303